Proceedings of the 11th ICPMG 2026
11th International Conference on Physical Modelling in Geotechnics
8-12 June 2026, Zurich, Switzerland

Centrifuge modelling of wave-seabed-pipe interaction using a hydraulic-driven type wave maker

Z.Y. Li, X.H. Wang, X.C. Chen, B. Zhu, D.Q. Kong
Zhejiang University, Hangzhou, China, deqiong_kong@zju.edu.cn (Corr. Author)

ABSTRACT: Waves present a significant threat to the stability of submarine pipes. To investigate wave-seabed-pipe interactions, a hydraulic-driven inflight wave maker device has been developed. This device is capable of generating regular periodic waves in water depths of 0.3 m at 50g, with the maximum frequency of 10 Hz. It serves as the preliminary research apparatus for the "Wave, Tsunami, and Gravity Flow Modelling Device" within China's major scientific and technological infrastructure facility "Centrifugal Hypergravity and Interdisciplinary Experiment Facility (CHIEF)". A series of wave-loading tests were conducted on seabeds with varying over-consolidated ratios. The pore pressure of seabeds nearby and far-from the model pipe was measured during tests. The main findings are as follows: (1) The instability mechanism of clayey seabeds is triggered by the degradation of shear strength under dynamic loading, rather than by the excess pore pressure reaching the effective self-weight stress; (2) Over-consolidated seabeds exhibit greater resistance to deformation under equivalent wave compared to the normally consolidated seabeds; (3) The residual pore pressure around the pipe exhibits a symmetrical distribution with higher magnitudes at the bottom than at the crown. The oscillatory pore pressure amplitude shows a markedly different pattern, with significantly larger values on the wave-facing side than the leeward side.

1 INTRODUCTION

With the ongoing exploitation of marine oil and gas resources, the scale of submarine pipeline installation has been expanding rapidly. Nevertheless, the marine environment is highly complex, and submarine pipelines are subjected to long-term cyclic loading induced by wave propagation. Studies have shown that as waves propagate in nearshore regions, they not only exert direct forces on marine structures but also induce cyclic wave pressure on the seabed foundation, which leads to the accumulation of excess pore pressure. This accumulation results in a reduction of effective stress and a consequent weakening or even loss of seabed strength. Therefore, the dynamic response of submarine pipelines under wave action has become a critical research focus in the field of marine geotechnical engineering.

Previous research on the dynamic response of seabeds under wave action has primarily focused on non-cohesive soils. From a theoretical perspective, early studies primarily employed Biot's consolidation theory and poroelastic models to investigate the instantaneous response of seabed soil under wave loading (Hsu and Jeng, 1994). For assessing the accumulation of excess pore pressure in the seabed under wave action, two approaches are commonly employed: one introduces a source term into the governing equations to represent the buildup of excess pore pressure (Jeng and Zhao, 2015), while the other utilizes elastoplastic constitutive models to compute corresponding plastic deformation and pore pressure accumulation (Ye et al., 2013).

Experimentally, wave flume tests are widely used. For example, Wang *et* al. (2020) carried out wave flume experiments to study changes in pore water pressure and effective stress in a sandy seabed under both regular and irregular waves. Chen et al. (2022) conducted wave flume tests to monitor the evolution of pore water pressure, soil strength, and particle characteristics, ultimately establishing an empirical formula to quantify the internal hardening force in consolidating silt. Sassa and Sekiguchi (1999) conducted centrifuge model tests using a flap-type wave generator mounted on a geotechnical centrifuge to investigate the liquefaction and reconsolidation of loose sandy seabeds under waves, providing new insights into physical modeling of geotechnical problems involving wave loads. Miyamoto et al. (2020) carried out a series of centrifuge tests investigating the instability of light pipeline and the liquefaction countermeasures for sandy seabeds under wave action.

Despite the widespread presence of soft clay in offshore areas and its poor engineering properties, such as high compressibility, low strength, and high sensitivity, the dynamic response of clayey seabeds under wave action has received significantly less attention than that of non-cohesive soils. Wit et al. (1997) conducted wave flume tests on the response of clayey seabeds, observing significant accumulation of excess pore pressure and seabed surface movement. However, Sassa & Sekiguchi (1999) pointed out that due to the limitations of lower stress levels in small-scale tests, extrapolating their conclusions to field conditions requires careful scrutiny. Thus, Wu et al. (2024) have used centrifuge testing to characterize excess pore pressure accumulation and strength evolution in cohesive seabeds under waves. However, the response of seabed around submarine pipelines under wave action was still a major research gap.

To address these gaps, this study employed centrifuge tests with a novel wave-modelling device to investigate wave–clayey seabed–pipe interaction. It specifically examined the effects of consolidation history and the presence of a pipeline on wave-induced seabed instability. The experimental program, conducted on seabeds with varying over-consolidation ratios, monitored shear strength of seabed as well as excess pore pressure in both the far-field and around the pipe, to elucidate the instability and reconsolidation behavior of the cohesive seabed surrounding the pipe.

2 METHODOLOGY

2.1 Inflight wave modelling device

The inflight wave-modelling device used in the tests was developed based on an existing wave generation device previously built at Zhejiang University (Zhu, 2023), which comprises four primary components: a wave-generating module, a wave-absorbing module, an inner soil tank, and a strong box, as shown in Fig. 1(a). The strong box has internal dimensions of 1.3 m (L) × 0.5 m (W) × 1.0 m (H), while the inner soil tank measures 0.55 m (L) × 0.27 m (W) × 0.48 m (H). The wave-generating module employs a flap-type wave paddle driven by a hydraulic cylinder. Throughout the tests, the servo-hydraulic system maintained real-time control of the wave paddle's frequency and displacement, thereby facilitating the generation of waves with designed periods and heights. The system has been successfully validated to generate regular periodic waves under 50g centrifugal acceleration. The wave-absorbing module operates on the principle of energy dissipation through turbulence and features an adjustable slotted partition. The porosity and placement of this partition are tailored to minimize wave reflection, thereby improving the system's operational performance. The model seabed was prepared using two distinct methods depending on the soil type: drained consolidated method for cohesive soils and sand-raining method for non-cohesive soils.

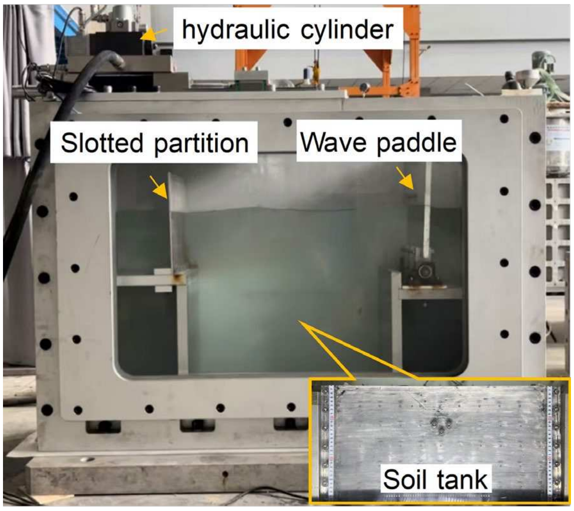

(a)

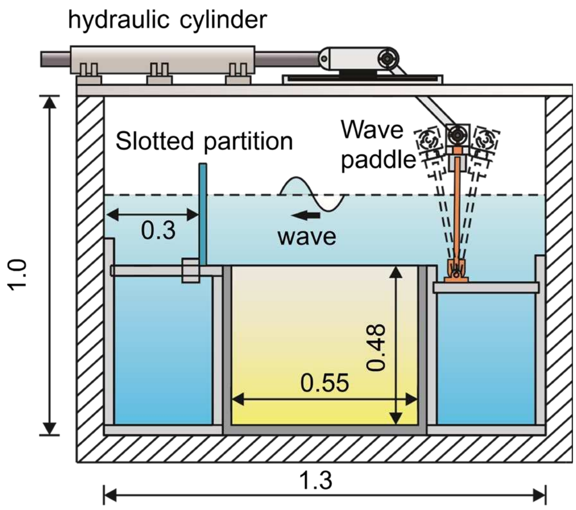

(b)

Figure 1. Wave loading device: (a) photograph; (b) schematic diagram

According to the flap-type wavemaker theory (Hughes, 1993), the wave height is calculated using Equation (1), which relates wave height to water depth and wave paddle displacement.

$$H = \frac{4S \times sinh(kh)}{sinh(2kh) + 2kh}\left[sinh(kh) + \frac{cosh(kh)}{kh}\right] \quad (1)$$

where H is the wave height, S is the water-surface wave paddle displacement, k is the wave number, and h is the depth of water.

According to linear wave theory, the wave pressure P_0 at the mudline is expressed as Equation (2):

$$P_0 = \frac{\rho_w ng \times H}{2 \times cosh(kh)} \quad (2)$$

where ρ_w denotes the fluid density (taken as 1000 kg/m³ in these experiments), and ng is the centrifugal acceleration.

A series of device tests were conducted at 50g, with the highest frequency reaching 10 Hz. The results demonstrate that the measured wave pressures under various conditions agree closely with theoretical predictions (Figure 2), thereby validating the accuracy of the apparatus in simulating waves.

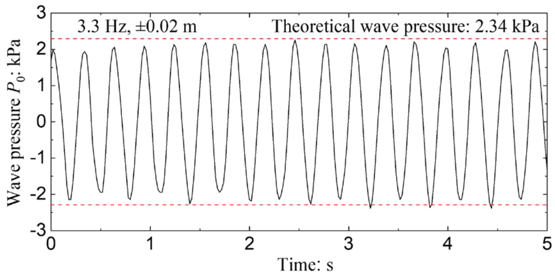

(a)

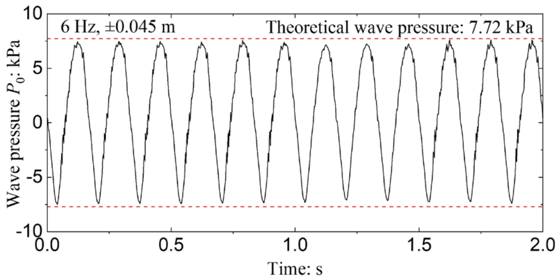

(b)

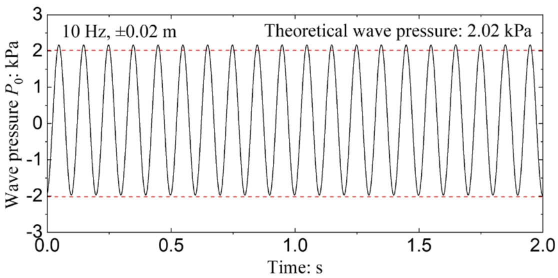

(c)

Figure 2. Comparison between measured and theoretical wave pressures under typical conditions: (a) 3.3Hz; (b) 6Hz; (c) 10Hz

2.2 Experimental setup

The centrifuge testing was performed on the ZJU-400 geotechnical centrifuge at Zhejiang University. This platform has a rotational radius of 4.5 m. In the present tests, the model seabed surface was located 3.92 m from the center of rotation.

2.2.1 Sensor and model pipe layout

Wave-induced seabed surface pressures and the internal pore pressure response were measured using an array of pore pressure transducers (PPTs; see layout in Figure 3(a)). A model pipe (D = 0.05 m) was buried to a depth of 2.5D and instrumented with four PPTs and four SPTs at 45° intervals around its circumference to monitor the soil-pipe interaction (Figure 3(b)). All PPTs shared a specification of -100–1000 kPa range, ±0.1% FS accuracy, and 2 kHz frequency response.

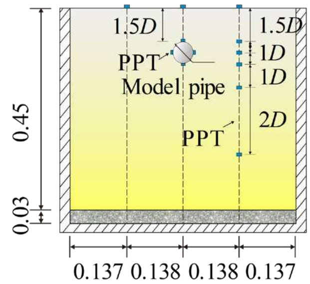

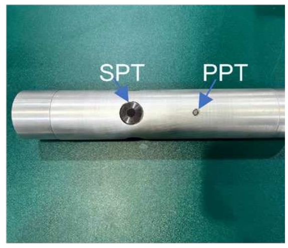

(a) *(b)*

Figure 3. Test setup: (a) layout of transducers; (b) photograph of model pipe

2.2.2 Preparation of model seabed

The model seabed was prepared by first placing a 0.03 m sand layer using the air-pluviation method, followed by placing a non-woven geotextile over it. The sand layer was saturated through a controlled upward flow of de-aired water, which raised the water table to just above the sand surface. Malaysian kaolin (properties summarized in Table 1) was selected as the clay material due to its well-characterized and reproducible behavior in previous studies (Goh, 2003). To form the clay layer, a fully saturated slurry was prepared by vacuum mixing dry kaolin with de-aired water to a water content of 160% for 24 h. The slurry was then placed over the geotextile, with a ~1 cm water head maintained above it to prevent evaporation. A four-vertical-drain system was installed, which connected the clay layer to the underlying sand layer (acting as a drainage boundary) and extended above the clay surface, to facilitate primary consolidation.

The testing program involved two seabeds consolidated in the centrifuge. Seabed 1 was formed from a 0.62 m high slurry and consolidated at 40g for 8 hours, resulting in a final thickness of 0.45 m that matched the surface of the soil tank, representing a normally consolidated seabed. Seabed 2 was prepared from a 0.79 m high slurry, consolidated at 50g for 8 hours, and then trimmed by 0.12 m from the top to achieve the same height as Seabed 1. The wave tests on Seabed 2 were conducted at 40g. This consolidation history produced an over-consolidated clay seabed. The over-consolidation ratio (OCR), defined as the ratio of pre-consolidation stress (σ'_c) to initial effective overburden stress (σ'_{v0}) at test acceleration, was calculated as OCR = 1.00 and OCR = 3.39 at z = -0.075 m for Seabeds 1 and 2, respectively. In previous studies, wave-induced instability has been shown to cause oscillatory movements of seabeds (Wit et al., 1997; Wu et al., 2024). To facilitate visual observation of such movements during the experiments, an artificial texture was created on the side of the model seabed using black sand prior to testing. A high-speed camera was then used to continuously monitor seabed changes throughout the tests.

Table 1. Properties of Malaysian kaolin clay (Goh, 2003)

Parameters	Value
Specific gravity, G_s	2.60
Liquid limit, ω_L: %	80
Plastic limit, ω_P: %	35
Coefficient of permeability, k: m/s	2.0e^{-8}
Coefficient of consolidation, C_v: m^2/year	40
Angle of internal fricition, φ: degrees	23
Void ratio of critical state, e_{cs}	2.221
Critical state parameter, M	0.9
Compression index, λ	0.244
Swelling index, κ	0.053

2.2.3 Test produces

As summarized in Table 2, all tests were performed at a 0.3 m model water depth and 40g centrifugal acceleration, corresponding to a prototype with a 12 m water depth and an 18 m thick seabed. Each test consisted of multiple wave loading and reconsolidation cycles. Test A involved loading the normally consolidated Seabed at a fixed frequency of 3.3 Hz (12 s prototype period) and achieving prototype wave heights of up to 1.2 m by modulating the paddle stroke. The wave loading phase lasted 300 s followed by a 900 s reconsolidation interval, equivalent to 3 h of prototype wave action and 16 days of prototype reconsolidation. Test B applied identical loading conditions to the over-consolidated Seabed to evaluate the OCR effect.

Table 2. Details of wave loading tests.

Test type	Test procedures		Time: min	P_0 kPa
Test A	E1	Loading	5	2.6
		Resting	1	
	E2	Loading	5	4.3
		Resting	15	
	E3	Loading	5	4.3
		Resting	15	
	E4	Loading	5	4.3
		Resting	15	
	E5	Loading	5	5.0
		Resting	15	
Test B	E1	Loading	5	2.6
		Resting	15	
	E2	Loading	5	4.5
		Resting	15	
	E3	Loading	5	5.1
		Resting	15	
	E4	Loading	5	5.1
		Resting	15	

3 RESULTS AND DISSCUSSIONS

Following the analytical approach of previous studies (Sassa and Sekiguchi, 1999; Miyamoto et al., 2023), the measured excess pore pressure (ΔP) data were separated into the residual pore pressure (u_{res}) and the oscillatory pore pressure (u_{osc}) for individual analysis.

Given the linear distribution of centrifugal acceleration with depth, the acceleration was set to 40g at two-thirds of the seabed depth (z = -0.333 m), following the approach of Wu et al (2024), to minimize the overall stress level error. Under this configuration, the centrifugal accelerations at the seabed surface and bottom are 38.53g and 42.95g, respectively, resulting in a centrifugal acceleration gradient of 9.82g (m^{-1}). Consequently, the effective self-weight stress was calculated based on this acceleration profile.

$$\sigma'_{v0} = \int_{3.92}^{3.92+z} 9.82g \times (\rho_{sat} - \rho_w) \times z dz \quad (3)$$

Where z is the depth within seabed; ρ_{sat} is the saturated density of seabed.

3.1 Wave-induced instability of seabed 1 (Test A)

Figure 4 shows the development of excess pore pressure (ΔP) at various depths within the far-field

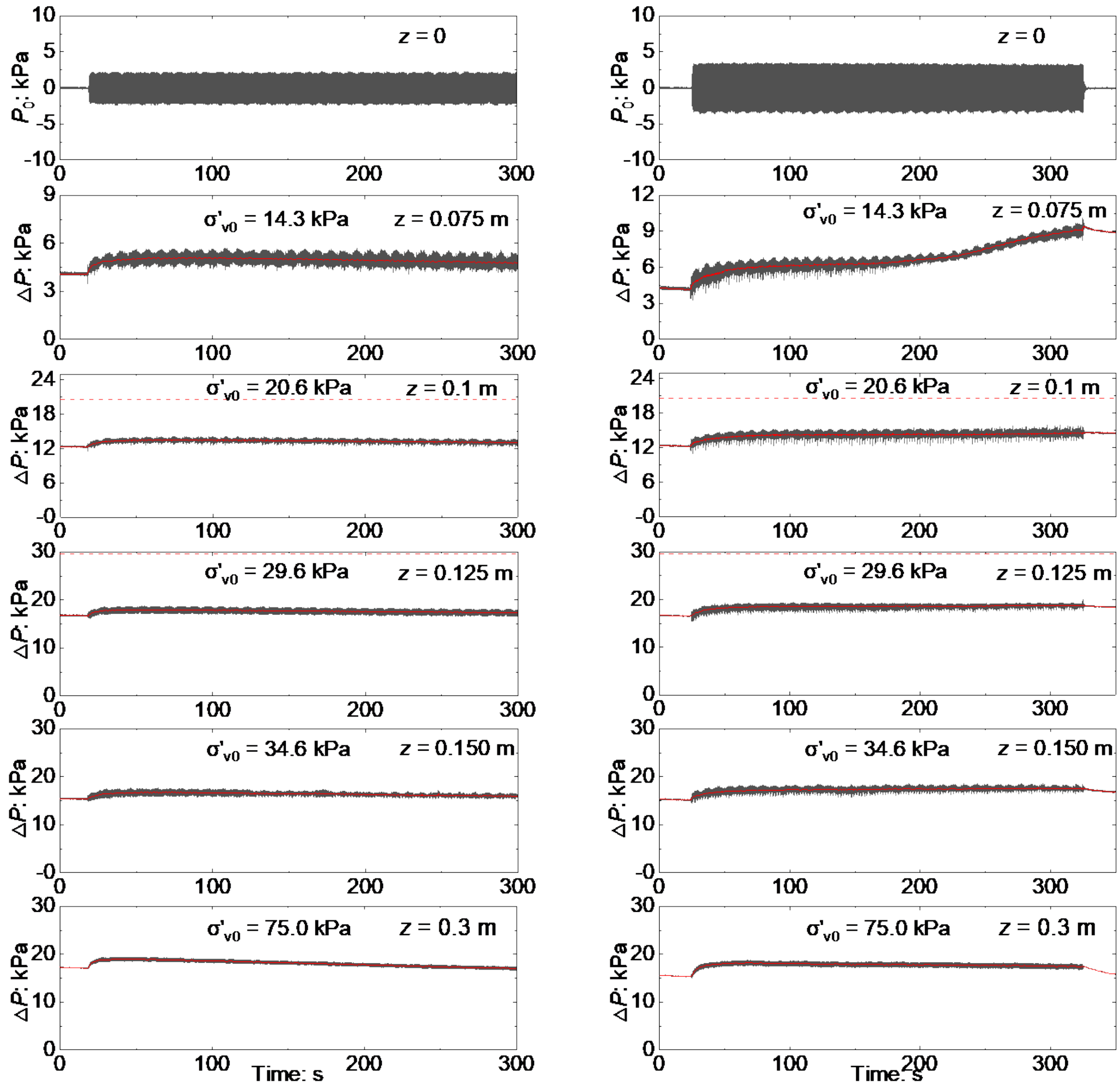

(a) *(b)*

Figure 4. The excess pore pressure acting in far-field seabed in Test A: (a) E1; (b) E2

seabed during the elastic (E1) and instability (E2) condition of Test A. The solid red lines represent the accumulated residual pore pressure obtained after signal processing. As shown in Figure 4(a), only slight ΔP accumulation occurred at all monitored depths under condition E1. In contrast, a significantly higher ΔP build up occurred at z = -0.075 m during the E2, as seen in Figure 4(b). Although the ΔP did not reach the effective self-weight stress, clear signs of seabed instability were observed at this depth under wave loading. These results suggest that the failure mechanism of cohesive seabeds fundamentally differs from that of sandy seabeds, which is likely attributable to a degradation of shear strength under the dynamic loading.

Figure 5(a) illustrates the depth-wise distribution of the maximum residual pore pressure (u_{res}) during Test A. The peak of u_{res} occurred at z = –0.125 m. After the initial seabed instability triggered in condition E2, subsequent wave loading conditions of comparable (E3 and E4) and higher (E5) intensity led to a progressive reduction in the maximum u_{res}. This trend indicates that after undergoing instability and reconsolidation, the seabed exhibited an increased stiffness and a significantly enhanced resistance to deformation.

Figure 5(b) shows the depth-dependent distribution of the normalized maximum amplitude of oscillatory pore pressure (u_{osc}). The theoretical analysis was conducted using the framework developed by Li &

Gao (2022), which provides a simplified equation for estimating the distribution of by incorporating the relative stiffness (R_k) between the soil skeleton and pore fluid over varying ranges. The measured maximum u_{osc} generally exhibits a decaying trend with depth, showing reasonable agreement with the theoretical predictions. Moreover, these amplitudes remain relatively stable across different loading conditions and exhibit no signs of the u_{osc} amplification characteristic of liquefaction in sandy seabeds (Sassa and Sekiguchi, 1999). These findings reinforce that the instability mechanism of cohesive seabeds is fundamentally distinct from the liquefaction behavior characteristic of sandy seabeds.

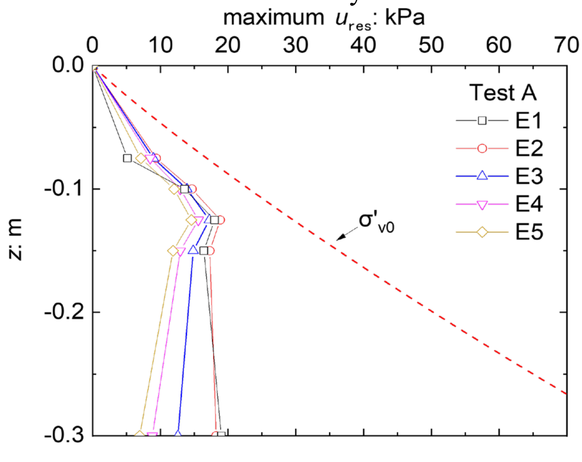

(a)

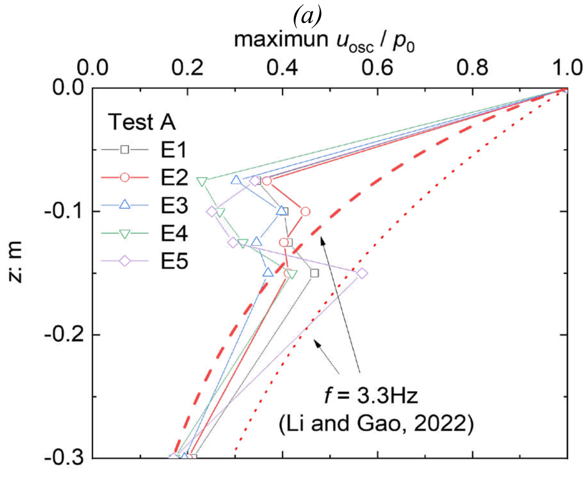

(b)

Figure 5. The excess pore pressure acting in far-field seabed in Test A: (a) maximum u_{res}; (b) maximum u_{osc}/P_0

Figure 6 presents the development of wave-induced pressure above the pipe and the accumulated excess pore pressure (ΔP) in the surrounding seabed during Test A. After low-intensity wave loading (E1), high-intensity waves (E2) caused a substantial increase in ΔP accumulation around the pipe. Notably, the ΔP at the pipe crown reached the effective self-weight stress. During subsequent wave loading cycles, the peak of ΔP gradually decreased, eventually falling below its initial value.

Figure 7 displays the distribution of the maximum residual pore pressure (u_{res}) around the pipe under different loading conditions. The maximum u_{res} is consistently elevated in the crown region relative to the pipe bottom, exhibiting a symmetrical pattern between the wave-facing (right) and leeward (left) sides. Consistent with the trend shown in Figure 6, a marked increase in u_{res} occurred from condition E1 to E2 in response to higher wave intensity, culminating in the crown pressure attaining the effective self-weight stress. In subsequent loading consitions, the reduction in maximum u_{res} at the crown was less pronounced compared to other circumferential positions.

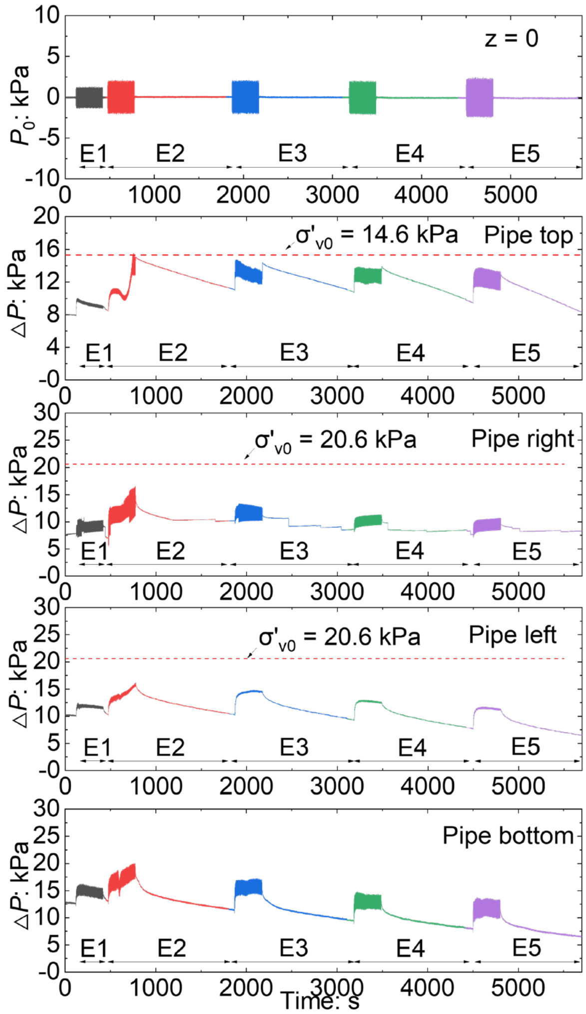

Figure 6. Time traces of wave pressure above pipe and excess pore pressure in the surrounding seabed

3.2 Effect of consolidation state

As described in Section 2.2.2, Test B involved wave loading on the over-consolidated Seabed 2. The seabed was first consolidated at 50g for 8 hours, after which a

0.12 m surface layer was removed to match the height of Seabed 1. This process was designed to simulate scouring-induced erosion at the prototype scale. Wave loading was subsequently applied under the same 40g and wave parameters as those in Test A.

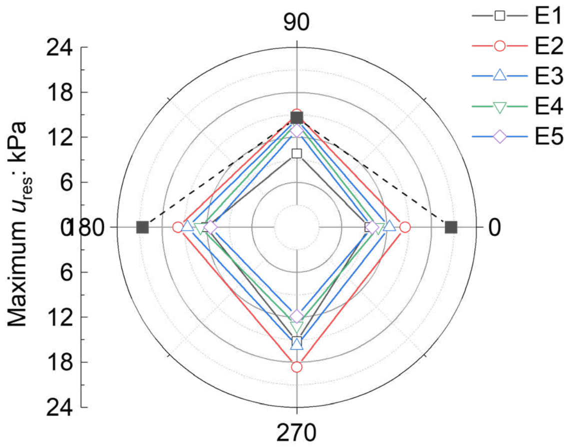

Figure 7. The maximum u_{res} acting around pipe in Test A

Figure 8 compares the distributions of the maximum residual pore pressure (u_{res}) in the far-field seabed for Test A and B. Under condition E1, both seabeds exhibited nearly identical distributions of maximum ures. However, the over-consolidated seabed in Test B showed no signs of instability, resulting in lower maximum u_{res} across various depths than those recorded in Test A under condition E2. This contrasting behavior indicates that the over-consolidated seabed possesses a greater capacity to resist deformation.

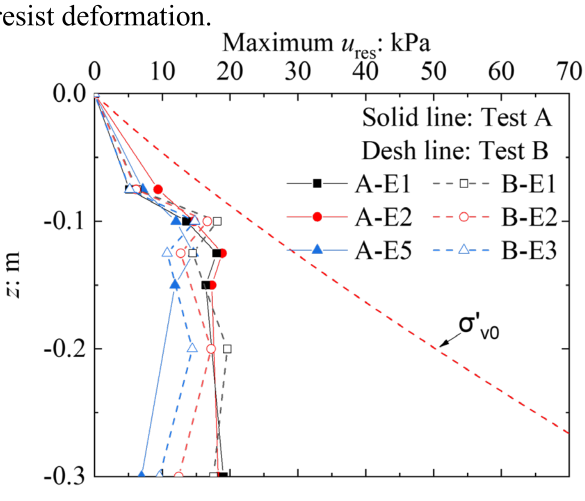

Figure 8. Comparison of maximum u_{res} in far-field seabed response between Test A and Test B

Figure 9(a) compares the distribution of maximum residual pore pressure (u_{res}) around the pipe for seabeds with different over-consolidation ratios (OCRs). The maximum u_{res} at the crown and bottom of the pipe in Test B were slightly higher than those in Test A under condition E1. Due to seabed instability in Test A during condition E2, the maximum u_{res} around the pipe were significantly greater than in Test B. Under subsequent higher-intensity wave loading, the maximum residual pore pressures at the crown and sides of the pipe in the normally consolidated seabed (Test A) remained higher than those in the over-consolidated seabed (Test B).

Figure 9(b) compares the distribution of the maximum amplitude of oscillatory pore pressure (u_{osc}) around the pipe for the two seabeds. Consistent with the trend observed for residual pore pressure, the maximum u_{osc} at the pipe crown under condition E2 and subsequent higher-intensity waves was notably smaller in Test B than in Test A. In contrast, at other locations around the pipeline—particularly on both sides—the distribution of oscillatory pore pressure amplitudes exhibited a pattern opposite to that observed at the crown.

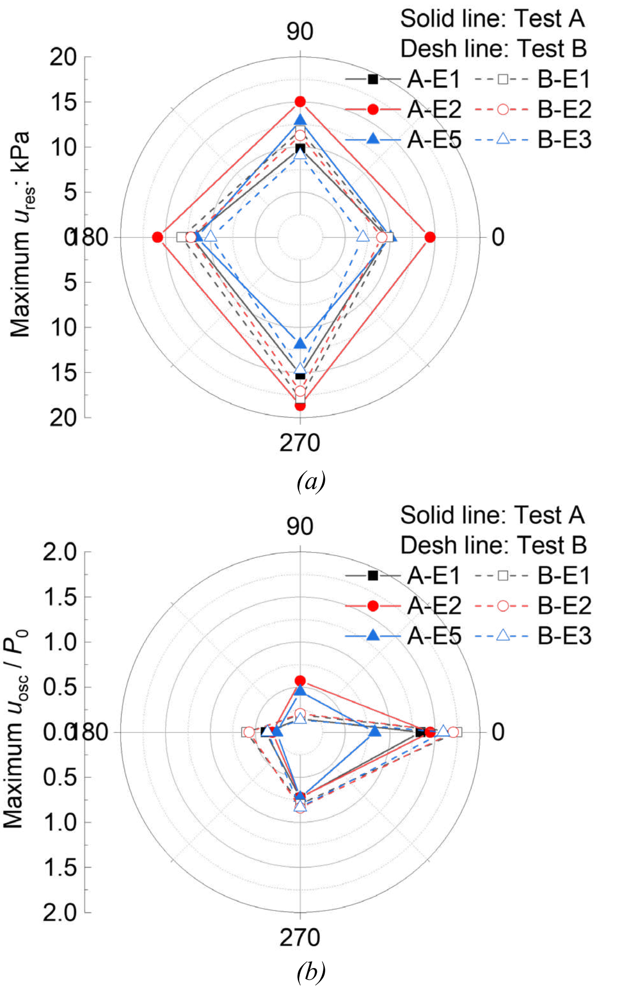

Figure 9. Comparison of seabed response around pipe between Test A and Test B: (a) maximum u_{res}; (b) maximum u_{osc}/P_0

4 CONCLUSIONS

This study presents the development of an inflight wave-modelling device and its implementation in centrifuge modeling to investigate the mechanism of wave–clayey seabed–pipe interaction. The principal findings are as follows:

(a) The developed inflight wave-modelling device is capable of stably generating waves at up to 10 Hz under 50g, thereby successfully replicating prototype conditions with a 15 m water depth and a 24 m thick seabed. Furthermore, the device accurately simulates wave-induced marine dynamic phenomena and the resulting seabed instability.

(b) Clayey seabeds under wave action are characterized by pronounced pore pressure accumulation. The instability mechanism of clayey seabeds differs from sand liquefaction, which is triggered by a degradation in dynamic strength rather than by the excess pore pressure reaching the effective self-weight stress.

(c) The over-consolidated seabed demonstrates a greater resistance to deformation under equivalent wave loading than the normally consolidated seabed, due to its pre-consolidation under higher stress.

(d) The residual pore pressure around the pipe exhibited a symmetrical distribution with higher magnitudes at the bottom than at the crown. In contrast, the oscillatory pore pressure amplitude showed a distinct pattern, with significantly larger values on the wave-facing side compared to the leeward side.

ACKNOWLEDGEMENTS

The authors are grateful for the financial support provided by the National Natural Science Foundation of China (Grant No. 51988101) and the Natural Science Foundation of Zhejiang Province (Grant No: LR23E090001).

REFERENCES

Hsu, J. R. C., and Jeng, D. S. (1994). Wave-induced soil response in an unsaturated anisotropic seabed of finite thickness. *International Journal for Numerical and Analytical Methods in 333. Geomechanics,* 18 (11): 785–807. https://doi.org/10.1002/nag.1610181104.

Jeng, D. S., Zhao, H. Y. (2015). Two-dimensional model for accumulation of pore pressure in marine sediments. *Journal of Waterway, Port, Coastal, and Ocean Engineering*, 141(3): 04014042. https://doi.org/10.1061/(ASCE)WW.1943-5460.0000282.

Ye, J. H., Jeng, D., Wang, R., and Zhu, C. (2013). Validation of a 2-D semi-coupled numerical model for fluid-structure-seabed interaction. *Journal of Fluids and Structures*, 42 (Oct): 333–357. https://doi.org/10.1016/j.jfluidstructs.2013.04.008.

Wang, X. W., Chen, S. G., Wang, R., and Zhang J. M. (2020). Large wave flume tests on wave-induced response of sandy seabed adjacent a water intake. *Ocean Engineering*, 195: 106709. https://doi.org/10.1016/j.oceaneng.2019.106709.

Chen, X. G., Zhang, F. P., Liu, X. X., Li, H., Zhang, X., Wei, Q., Wang, L. Z., Tang, H. P., Wei, J, K., Li, K. H. (2022). Evolution process and hardening mechanism of consolidated silt in silty seabed subject to waves. *Applied Ocean Research*, 125: 103214. https://doi.org/10.1016/j.apor.2022.103214.

Sassa, S., and Sekiguchi, H. (1999). Wave-induced liquefaction of beds of sand in a centrifuge. *Géotechnique*, 49 (5): 621–638. https://doi.org/10.1680/geot.1999.49.5.621.

Miyamoto, J., Sassa, S., Ito, H., Tsurugasaki, K., and Sumida, H. (2023). Wave-Induced Liquefaction and Stability of Suction Bucket Foundation in Drum Centrifuge. *Journal of Geotechnical and Geoenvironmental Engineering*, 149 (4): 04023013. https://doi.org/10.1061/JGGEFK.GTENG-11247.

Wit, P. J., Kranenburg, C. (1997). The wave-induced iquefaction of cohesive sediment beds. *Estuarine, Coastal and Shelf Science*, 45(2): 261−271. https://doi.org/10.1006/ecss.1996.0184.

Wu, L. Y., Kong, D. Q., Zhu, B., Chen, R. P., and Chen, Y. M. (2024). Centrifuge modelling of wave-induced seabed response in clay. *Géotechnique,* 74 (2): 103–115. https://doi.org/10.1680/jgeot.21.00105.

Zhu, J. S. (2023). *Centrifuge and numerical modelling on wave-seabed-pipe interaction*. PhD thesis, [In Chinese] China: Zhejiang University.

Hughes, S. A. (1993). Physical Models and Laboratory Techniques in Coastal Engineering. *Singapore: World Scientific*.

Goh, T. L. (2003). *Stabilisation of an excavation by an embedded improved soil layer*. PhD thesis, Singapore: National University of Singapore.

Li, C. F., and Gao, F. P. (2022). Characterization of spatio-temporal distributions of wave-induced pore pressure in a non-cohesive seabed: Amplitude-attenuation and phase-lag. *Ocean Engineering* 253 (Jun): 111315. https://doi.org/10.1016/j.oceaneng.2022.111315.